

Metamagnetism of few layer topological antiferromagnets

C. Lei,¹ O. Heinonen,² A.H. MacDonald,¹ and R. J. McQueeney^{3,4}

¹*Department of Physics, The University of Texas at Austin, Austin, TX 78712*

²*Argonne National Laboratory, Argonne, IL USA*

³*Ames Laboratory, Ames, IA, 50011, USA*

⁴*Department of Physics and Astronomy, Iowa State University, Ames, IA, 50011, USA*

(Dated: February 24, 2021)

MnBi₂Te₄ (MBT) is a promising antiferromagnetic topological insulator whose films provide access to novel and technologically important topological phases, including quantum anomalous Hall states and axion insulators. MBT device behavior is expected to be sensitive to the various collinear and non-collinear magnetic phases that are accessible in applied magnetic fields. Here, we use classical Monte Carlo simulations and electronic structure models to calculate the ground state magnetic phase diagram as well as topological and optical properties for few layer films with thicknesses up to six septuple layers. Using magnetic interaction parameters appropriate for MBT, we find that it is possible to prepare a variety of different magnetic stacking sequences, some of which have sufficient symmetry to disallow non-reciprocal optical response and Hall transport coefficients. Other stacking arrangements do yield large Faraday and Kerr signals, even when the ground state Chern number vanishes.

INTRODUCTION

MnBi₂Te₄ (MBT) is a promising platform for the development of unique devices based on topological electronic bands [1–28]. The utility of MBT is consequence of its natural layered structure, which consists of stacks of ferromagnetic (FM) septuple layers (SLs) with out-of-plane magnetization and with inverted electronic bands with non-trivial topology [1–3]. There is great interest in manipulating the sequence of magnetic and topological layers as a means to control phenomena related to the band topology [9]. Bulk MBT adopts a staggered antiferromagnetic (AF) stacking of the FM SLs [3, 10, 12, 18], providing the first realization of an AF topological insulator, which is predicted to host unique axion electrodynamics [29, 30]. Weak interlayer magnetic interactions across the van der Waals gap and uniaxial magnetic anisotropy allow for facile control of the magnetic structure. For example, a bulk Weyl semimetallic phase is predicted when all FM layers in MBT are co-aligned with a small applied magnetic field [9, 15, 16].

Perhaps the most exciting opportunity in MBT materials is the possibility of developing thin film devices with precisely controlled magnetic stacking sequences. In this context, devices with even and odd numbers of AF stacked layers offer qualitatively different topological phase possibilities [11, 23, 28, 31–33]. An odd number of magnetic layers necessarily has partially compensated magnetization that is beneficial for the observation of the quantum anomalous Hall (QAH) effect [11]. On the other hand, fully compensated magnetization occurs in even layer devices in the absence of an applied magnetic field and provides an ideal platform to search for axion insulators with quantized magnetoelectric coupling [13, 23]. However, there are also much richer possibilities in both odd or even layer samples [33], since the application of a

magnetic field can result in different collinear magnetic stackings with partially compensated magnetization, or even to non-collinear (canted) magnetic phases. Here, we consider the possibility to stabilize such phases and the potential for realizing unique topological phases in this scenario.

The magnetization behavior of AF magnetic multilayers displays rich metamagnetic behavior with features, such as surface spin-flop transitions, that are not observed in bulk AFs [34, 35]. This complex behavior is a consequence of competition between single-ion anisotropy, interlayer magnetic exchange, and Zeeman energy. For topological materials, whether the symmetry of different magnetic layer stacking sequences can affect the topological properties of the bands is an open question. For example, collinear metamagnetic phases with the same net magnetization can result from magnetic layer stackings that may or may not break mirror symmetry (\mathcal{M}). Here we use classical Monte Carlo simulations to show that it is generally possible to tune in different stacking sequences with distinct symmetries. What's more, we find that realistic values of the single-ion anisotropy and exchange place MBT close to this tunability regime. Finally, we discuss the topological properties of accessible field-tuned states and strategies to identify them experimentally.

MONTE CARLO SIMULATIONS OF BULK MNBI₂TE₄

The spin lattice of MBT consists of triangular FM layers which are stacked in a close-packed fashion along the direction perpendicular to the layers. Interlayer interactions are AF, resulting in the zero-field A-type ground state [see Fig. 1(a)]. Magnetization and neutron diffraction experiments find Mn moments oriented

perpendicular to the layers consistent with uniaxial magnetic anisotropy [18]. These features suggest that a simple spin model can be used to study the magnetization behavior of MBT in an applied magnetic field

$$H = J' \sum_{\langle ij \rangle ||} \mathbf{S}_i \cdot \mathbf{S}_j + J \sum_{\langle ij \rangle \perp} \mathbf{S}_i \cdot \mathbf{S}_j - D \sum_i S_{i,z}^2 - g\mu_B \mathbf{H} \cdot \sum_i \mathbf{S}_i. \quad (1)$$

Here, \mathbf{S}_i is the Mn spin at site i ($S = 5/2$), $J' < 0$ is the intralayer FM exchange, $J > 0$ is the interlayer AF exchange and D is the uniaxial single-ion anisotropy. Each Mn ion has six interlayer and intralayer nearest-neighbors ($z = 6$). A representative and consistent set of magnetic coupling parameter values for MBT have been obtained from magnetization [18] and inelastic neutron scattering experiments [17]; $SJ' = -0.35$ meV, $SJ = 0.088$ meV, and $SD = 0.07$ meV.

Using these nominal values, classical Monte Carlo (MC) simulations on bulk and few layer MBT systems have been performed using both UppASD [36] and Vampire [37] software packages. MC simulations are first performed on bulk MBT with a $21 \times 21 \times 12$ system size (15876 spins) with periodic boundary conditions. MC simulations are run with the field pointed perpendicular to the layers using 50000 MC steps per field. To account for hysteresis and history dependence, we begin the simulations with the field polarized state at $H = 10$ T and ramp the field down in equal steps, using the final state from the previous field as the initial state for the current field.

Figure 1(b) summarizes typical MC simulation results for bulk MBT that reveal a Néel temperature of 22 K and magnetization curves with field-polarized saturation fields ($\mu_0 H_{ab}^{sat} = 10.3$ T and $\mu_0 H_c^{sat} = 7.9$ T), and a spin-flop field ($\mu_0 H_{SF} = 3.7$ T), in agreement with bulk measurements [10, 12, 18]. The hysteresis of the spin-flop transition is noticeably absent in the experimental data of bulk single-crystals, which suggests that the spin-flop transition in real crystals does not occur by coherent layer rotation and could occur instead by surface nucleation [38].

For a general bulk uniaxial AF, critical values of the ratio D/zJ determine the magnetization behavior when the field is applied along the c -axis. Only three phases are possible, the AF phase, the canted spin-flop phase (SF), and the field-polarized phase (FM). For relatively weak anisotropy $D/zJ < 1/3$, a first-order spin-flop transition phase is expected, followed by a second-order transition to the field polarized state (AF \rightarrow SF \rightarrow FM). The nominal MBT parameters yield $D/zJ \approx 0.13$ which is within the spin-flop regime. For dominant single-ion anisotropy $D/zJ > 1$, the virgin AF state is swept out by a weak applied field and a FM hysteresis loop develops. This behavior is observed in MnBi_4Te_7 , in which the addition of a non-magnetic Bi_2Te_3 spacer between MnBi_2Te_4 layers dramatically weakens the interlayer magnetic exchange

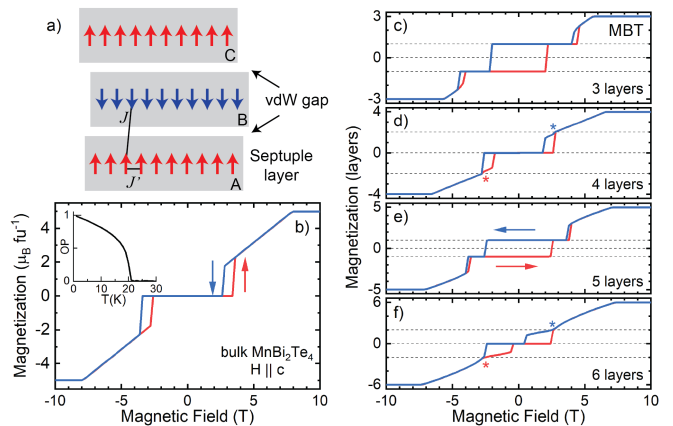


Figure 1. (a) Schematic magnetic layer structure of MBT in the crystallographic unit cell with close-packed stacking of septuple layers. The intralayer (J') and interlayer (J) magnetic interactions are indicated. The gray shaded boxes indicate the full septuple layers separated by a van der Waals gap. (b) Monte Carlo simulations of MBT with field applied perpendicular to the Mn layers. Inset shows the order parameter (OP) of the staggered A-type AF order as a function of temperature. (c)-(f) Monte Carlo simulations of the magnetization of 3, 4, 5, and 6 layer MBT, respectively, using the nominal Heisenberg parameters. For $N = 4$ and 6, the "x" indicates an additional phase transition.

[39, 40]. In the intermediate regime $1/3 < D/zJ < 1$, the AF \rightarrow FM transition occurs directly (a spin-*flip* transition), whereas the field-reversed transition goes through the spin-flop regime (FM \rightarrow SF \rightarrow AF).

FIELD-TUNED FEW-LAYER MAGNETIZATION

We now consider the behavior of the magnetization in thin film samples consisting of N magnetic layers, with $N = 3, 4, 5$ and 6. The magnetic phase diagram of the N -layer systems is much more complex than the bulk phase diagram because regions of stability exist (as described in detail below) that correspond to collinear magnetic phases with partially compensated magnetization (ferromagnetic phases). In this respect, significant differences occur between odd or even layer systems because the net magnetization cannot be fully compensated in odd layer films. Fig. 1 (c)-(f) shows the magnetization for $N = 3, 4, 5$, and 6-layer MBT obtained from MC simulations using a 11×11 system size for the basal layer and the nominal MBT Heisenberg parameters. Select simulations with a 21×21 basal layer produced no significant changes in the magnetization sweeps.

For $N = 3$ and 5 layer simulations with the nominal MBT parameters, we find the expected FM hysteresis loop corresponding to the magnetization of a single uncompensated layer ($M = \pm 1$). In addition, we find a hysteretic spin-flop-like transition from the $M = \pm 1$ phase to the fully polarized FM phase. For $N = 4$ and $N = 6$, magnetization curves resemble bulk MBT with a AF \rightarrow

SF \rightarrow FM sequence of transitions. However, one notices evidence for an additional transition [indicated with a "*" in Fig. 1(d) and (f)] within the spin-flop phase near 3 T. As we will show below, this transition demonstrates that the nominal parameters of MBT are close to a critical point in the phase diagram at which the $M = 2$ collinear phase becomes stable. We note that experimental evidence exists for $M = 2$ magnetization plateaus in the $N = 4$ and 6-layer films based on reflective magnetic circular dichroism experiments [32, 33]. The experimental magnetization results in Refs. [32, 33] are analyzed using numerical methods similar to the Mills model [41] described below.

To explore the nature of this critical point and parameter regimes beyond the nominal values chosen to represent MBT, we calculated the phase diagrams for the 3, 4, 5, and 6-layer systems as a function of field and the single-ion anisotropy parameter, as shown in Fig. 2. Generally, these phase diagrams show regions of collinear magnetism separated by non-collinear (spin-flop-like) phases. For the largest uniaxial anisotropy values, the system approaches the behavior of a finite Ising chain where successive first-order transitions occur via single-layer spin-flips. We label the collinear ground state phases as; AF ($M = 0$, $N = \text{even}$ only), Mn ($M = n$, with $n - 1$ broken AF bonds), and FM ($M = N$, field-polarized with all AF bonds broken). Their time-reversed states are indicated by a bar (eg. $\overline{M2}$) and states that have identical ground state energies within our model, when they occur, are differentiated by a prime symbol (eg. $M2'$, $M2''$). Metastable excited states, when they occur, are labeled with an asterisk (eg. $M0^*$).

METAMAGNETIC STATES

The distinct collinear ground states that occur for $N = 3$ and $N = 4$ are illustrated in Fig. 3(a) and (b). For $N = 4$, the MC phase diagram in Fig. 2(b) is consistent with the phase boundaries, critical points, and metastability limits obtained using the Mills model [35, 41]. As expected, slightly increasing D from the nominal MBT value of $SD = 0.07$ meV stabilizes the $M2$ collinear phase, replacing the inflection in Fig. 1(d) with a magnetization plateau. Analysis of 4-layer Mills model reveals that this critical point occurs at $(SD, \mu_0 H)_\beta = (0.082 \text{ meV}, 3.59 \text{ T})$ [35], corresponding to a critical ratio of $D/zJ = 0.16$.

For odd thin film thicknesses ($N = 3$ and 5), the magnetization sequence at low D/zJ reveals $M1$ and $\overline{M1}$ phases that form a hysteresis loop. For $N = 5$, larger D/J reveals two $M3$ states occur, labelled as $M3'$ and $M3''$ in Fig. 3(c), which have identical energies in our model but are distinguished by the presence ($M3'$) or absence ($M3''$) of mirror symmetry. Analysis of the sublattice magnetization from our simulations shows that only

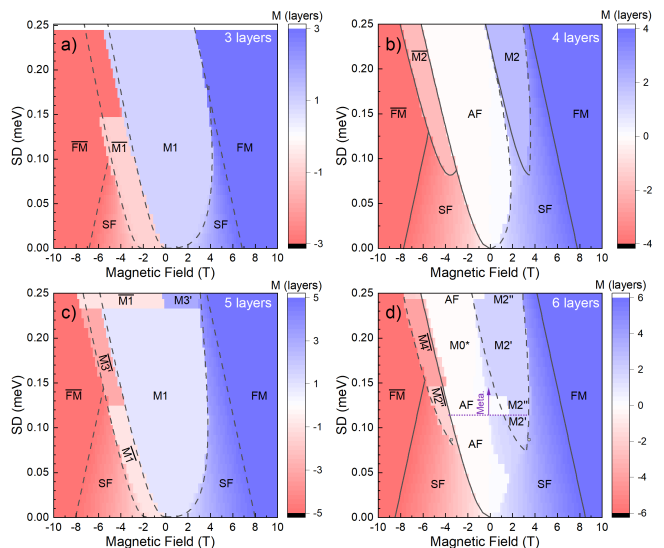


Figure 2. Phase diagrams obtained by MC simulation showing the layer magnetization of a uniaxial layered antiferromagnet *vs.* magnetic field applied perpendicular to the layers and single-ion anisotropy strength (SD) for (a) 3 layers, (b) 4 layers, (c) 5 layers and (d) 6 layers. Simulations start in the FM phase at 10 T and the field strength is reduced in equal steps of 0.2 T to -10 T. The solid lines are phase boundaries and metastability limits obtained from the Mills model, the dashed lines are guides to the eye. Collinear phases are labeled as described in the text. For $N = 6$, panel (d) indicates a metastability limit below which only the $M2''$ phase is stabilized out of the SF phase.

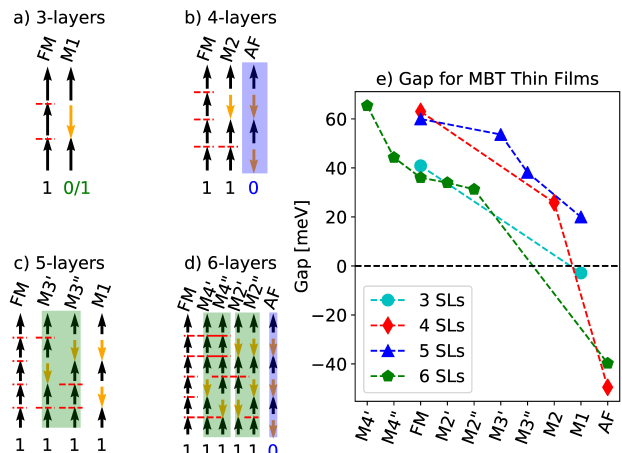


Figure 3. Possible collinear magnetic ground states for $N = 3, 4, 5$, and 6-layer systems, labeled as either FM, AF or Mn , where n is the uncompensated net layer magnetization. Red dashed lines indicate broken AF bonds that cost an exchange energy of $3J$ each. Shaded green rectangles enclose degenerate states with the same magnetization, but different stacking sequences indicated by the prime symbol. Shaded blue rectangles enclose the states with odd-parity magnetic configuration (i.e. \mathcal{TM} symmetrized magnetic configuration, with \mathcal{T} time-reversal and \mathcal{M} mirror symmetry). The integers below each state denote their Chern numbers calculated from a the simplified Dirac-cone model and (e) are the calculated band gaps *vs.* the magnetic stacking sequences of few-layer MBT thin films.

the mirror symmetric $M3'$ phase appears in the range of D/zJ studied.

Much more interesting and complex behavior is obtained for thin films with $N = 6$, where collinear phases appear that have equal uncompensated magnetizations but different symmetries. These phases appear beyond the critical point, as in the $N = 4$ case, which is estimated to be $(SD, \mu_0 H)_\beta = (0.084 \text{ meV}, 3.46 \text{ T})$ from the 6-layer Mills model [35] with $D/zJ = 0.16$. Close to the critical point, two different $M2$ phases appear at positive and negative fields, labeled $M2'$ and $M2''$ as shown in Fig. 3(d). The mirror symmetric $M2'$ phase has a single broken AF bond in the center of the stack, and is found emerging out of the spin-flop phase ($\text{FM} \rightarrow \text{SF} \rightarrow M2'$). The mirror symmetry broken $M2''$ has a broken AF bond on the surface and is always stabilized out of the AF state ($\text{AF} \rightarrow M2''$).

The preference for the $\text{AF} \rightarrow M2''$ transition over the $\text{AF} \rightarrow M2'$ transition can be understood from metastability arguments related to the barrier height for layer flips that is determined primarily from the uniaxial anisotropy. The $\text{AF} \rightarrow M2''$ transition requires a coherent spin flip of the surface layer only, whereas $\text{AF} \rightarrow M2'$ requires three layer flips. From the FM side, both $M2'$ and $M2''$ require two layer flips and, for this reason, either phase is likely to appear within our simulations when $D/zJ \gtrsim 0.2$, as indicated by the purple dotted line in Fig. 2(d). Due to its larger barrier height, $M2'$ has a lower metastability field to enter the AF phase than $M2''$ as the field is reduced. To illustrate the metastability limit, Fig. 4(a) and 4(b) show that repeated simulations in which the field is reduced starting the FM phase will always generate $M2'$ with $SD = 0.11 \text{ meV}$, whereas either $M2'$ or $M2''$ may appear with $SD = 0.12 \text{ meV}$. This metastability limit at intermediate D/zJ originates from the intervening spin-flop phase that selectively lowers the barrier to the mirror symmetric $M2'$ phase when layers 2 and 5 have a large spin-flop angle, as shown in Fig. 4(c)–(e).

At large D/zJ , metastability issues with the MC simulations reveal that even excited states (such as the $M0^*$ state with stacking sequence up-down-up-down-down-up) may be trapped in a local minimum. The occurrence of the $M0^*$ phase is dependent on whether the $M2'$ or $M2''$ phase appears when lowering the field out of the FM phase. As described above, when the $M2''$ phase appears, the AF phase is favored since only a spin flip of the surface layer is required. When the $M2'$ phase appears, transition to the AF phase has a high barrier requiring three layer spin flips. It is therefore more likely for the $M2'$ phase to transition to the metastable $M0^*$ state in which the barrier height is set by a single layer flip. While this regime is not applicable for MnBi_2Te_4 , where $D/zJ \approx 0.13$, it may be applicable to MnBi_4Te_7 in which non-magnetic Bi_2Te_3 spacer layers dramatically reduce J .

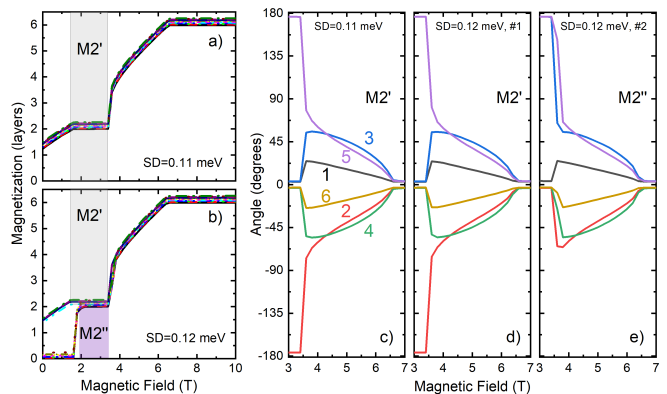


Figure 4. (a)-(b) Twelve MC simulations for $N = 6$ repeated under identical starting conditions near the metastability limit for formation of the $M2'$ phase. Curves have a slight vertical offset for clarity. (a) For $SD = 0.11 \text{ meV}$, only the $M2'$ phase appears. (b) For $SD = 0.12 \text{ meV}$, either the $M2'$ or $M2''$ phase appears. (c)-(e) show the evolution of the magnetization angle for each layer for different simulations. (c) For $SD = 0.11 \text{ meV}$, which is below the metastability limit, the angle of layers 2 and 5 in the spin-flop phase approaches 90° before flipping into the $M2'$ phase. For $SD = 0.12 \text{ meV}$, different simulations (labeled #1 and #2) result in either (d) $M2'$ with layers 2 and 5 flipping or (e) $M2''$ with layers 3 and 5 flipping.

TOPOLOGICAL AND OPTICAL PROPERTIES

A very interesting question is how the stacking sequence of the magnetic layers in MBT thin films and the possible concomitant breaking of symmetries affect observable electronic properties, particular those related to the topological classification of the electronic structure. To gain insight, we used a simple model of stacked 2D Dirac metals, 2 for each MBT layer, to calculate the band structure, Chern numbers, and magneto-optical responses of different magnetic states. Previous work [9] has shown that with appropriate coupling between the Dirac metals, models of this type provide a reasonable description of MBT thin films.

As summarized in Fig. 3, we find that for $N > 3$ all states have unity-magnitude Chern numbers whenever they have uncompensated magnetization, signaling non-trivial topological states. The calculated Chern numbers are listed below each state. Odd $N > 3$ systems are therefore always QAH insulators. The $N = 3$ $M1$ state is labelled as $0/1$ because it has an extremely small gap and can be on either side of the topological phase, transition depending on exchange interaction parameters and on the residual electric field that is likely to be present in any MBT thin films [42]. The gaps of the various magnetic states we have identified are shown in Fig. 3(e), with a negative sign attached to distinguish cases in which the Chern number is 0 from cases in which the Chern number is 1. The QAH gaps are generally larger for FM magnetic configurations for MBT thin films, except for the $M4'$ and $M4''$ states of $N = 6$ films, which have larger gaps than

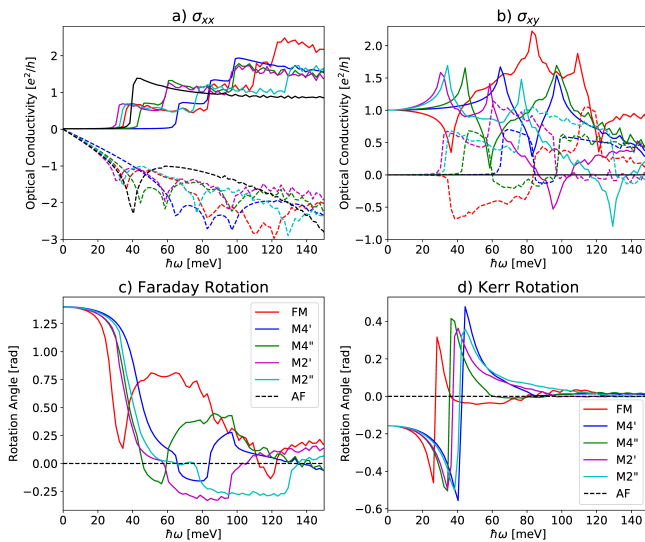


Figure 5. Non-reciprocal optical response in 6-layer MBT thin films. Panels (a) and (b) show plots of optical longitudinal (σ_{xx}) and Hall (σ_{xy}) conductivities *vs.* optical frequency calculated from the Kubo-Greenwood formula using the simplified Dirac cone electronic structure model. In these plots the solid curves show the real part of a conductivity tensor element while the dashed curves show the imaginary part. Different colors show results for different metamagnetic states. The correspondence between color and metamagnetic state is repeated in (c) and (d), in which the Faraday and Kerr rotation angles in $N=6$ thin films are plotted *vs.* optical frequency.

the M6 state.

Symmetries play an important role in film electronic properties. We define odd-parity magnetic configurations as ones that have the property that the magnetic moments reverse upon layer reversal (i.e. \mathcal{TM} symmetrized magnetic configurations with \mathcal{T} the time-reversal operator). Odd-parity magnetic configurations can be read from the cartoons enclosed with shaded blue rectangles in Fig. 3, and include even- N AF configurations. Whenever the magnetic configuration has odd parity, the band Hamiltonian is invariant under the product of time-reversal symmetry \mathcal{T} and inversion symmetry \mathcal{I} . (Note that the spin-orbit coupling terms in coupled Dirac-cone model on the top and bottom surfaces of each septuple layer differ by a sign.) For many observables, the consequences of \mathcal{TI} invariance are the same as the consequences separate \mathcal{T} and \mathcal{I} invariance. For example, \mathcal{TI} invariance implies that the Berry curvature $\Omega_n(\mathbf{k}) = -\Omega_n(\mathbf{k}) = 0$. The Berry curvature therefore vanishes identically and a generalized Kramer's theorem implies that all bands are doubly degenerate. It follows that the Chern number vanishes for odd-parity magnetic configurations.

$N = 6$ layer thin films host a richer variety of metamagnetic states. We find that all magnetic configurations with a non-zero net spin magnetization (FM, M2'/M2'' or M4'/M4'') have total Chern number equal to 1 and

are therefore QAH insulators. The states cannot be distinguished by performing DC Hall effect measurements. Those properties that are not quantized are distinct for each of these states however. For example, the Berry curvature has a different dependence on momentum in each case, although the total Chern number is always equal to one. As shown in Fig. 5, their optical conductivities differ at finite frequencies. In Fig. 5 (a) and (b) the real and imaginary part of longitudinal optical conductivities $\sigma_{xx}(\omega)$ and transverse optical conductivities $\sigma_{xy}(\omega)$, calculated using the Kubo-Greenwood formula, [43, 44] are shown. In these plots solid curves represent the real part of the conductivity ($\Re\sigma_{xx/xy}$) while dashed curves represent the corresponding imaginary parts ($\Im\sigma_{xx/xy}$). Different colors are used to represent different metamagnetic states. The same colors are used for the implied frequency-dependent Faraday and Kerr rotation angles in Fig. 5 (c) and (d). It follows that external magnetic fields drive the 4-layer and 6-layer thin films from their axion insulator states to M2, M2' or M2'' Chern insulators.

In the DC limit, all optical conductivities vanish except for $\Re\sigma_{xy}$ in the case of a QAH insulator. $\Re\sigma_{xx}$ and $\Im\sigma_{xy}$ have peaks when the optical frequencies exceeds the two-dimensional band gaps of the thin film. $\Im\sigma_{xx}$ and $\Re\sigma_{xy}$ are, on the other hand, non-zero for frequencies in the thin-film gaps. The frequency dependence of $\Re\sigma_{xy}$ and $\Im\sigma_{xy}$ in the FM states differs from that of other magnetic states in that $\Re\sigma_{xy}$ initially decreases with frequency and $\Im\sigma_{xy}$ is negative below the band gap. This abnormal behavior is caused by the negative Berry curvature around the Γ point in the 2D-band structure.

The optical conductivity tensor components can be converted to frequency-dependent Faraday and Kerr rotation angles commonly measured in experiment. The Faraday and Kerr rotation angles are the relative rotations of left-handed and right-handed circularly polarized light[45] for transmission and reflection respectively, and these can be connected to the optical conductivity by combining electromagnetic wave boundary conditions and Maxwell equations. The Faraday and Kerr rotation angle *vs.* optical frequency for various metamagnetic states of 6-layer thin film are shown in Fig. 5(c) and (d) correspondingly, from which we see that the optical responses of all metamagnetic states with the same Chern number are indistinguishable in the DC limit. As frequency increases, the Faraday and Kerr rotation angles of different metamagnetic states differ substantially. It follows that different metamagnetic states can be distinguished magneto-optically.

DISCUSSION

In our studies, we have identified the metamagnetic states that can be induced in MBT thin films with up

to $N = 6$ septuple layers by applying external magnetic fields. For $N = \text{odd}$ and larger than 3, all MBT thin films states are QAH insulators. For even- N , the ground states are axion insulators in the absence of an external magnetic field. Metamagnetic states that are Chern insulators can be induced by applying external magnetic field provided that the single-ion magnetic anisotropy is large enough compared with the interlayer exchange interactions. Both M2 and M4 states are Chern insulators with QAH gaps comparable to those of the FM state, and appear at a much smaller magnetic fields. These metamagnetic states are not distinguished in transport experiment since they all have the same Chern number as the FM state. However, They are distinguished by their magneto-optical Kerr and Faraday rotation angles.

Thicker films, especially for even-layer systems and for the thin films with high Chern number FM states (that is $N = 9$ layers thin or thicker), await further exploration. Interesting questions arise when the thickness increases: is it possible, for example, to have a high-Chern-number state at a weaker magnetic field? For MBT thin films the magnetic anisotropy seems to be comparable with the interlayer exchange interaction, it may therefore be interesting to explore other intrinsic magnetic topological insulators that have relative larger magnetic anisotropy to induce more metamagnetic states, or to find tools, such as electric field, that may increase the magnetic anisotropy.

ACKNOWLEDGEMENTS

RJM and OH were supported by the Center for Advancement of Topological Semimetals, an Energy Frontier Research Center funded by the U.S. Department of Energy Office of Science, Office of Basic Energy Sciences, through the Ames Laboratory under Contract No. DE-AC02-07CH11358. CL and AHM were supported by the Army Research Office under Grant Number W911NF-16-1-0472. OH gratefully acknowledges the computing resources provided on Bebop and Blues, high-performance computing clusters operated by the Laboratory Computing Resource Center at Argonne National Laboratory.

APPENDIX

-
- [1] S. V. Eremeev, M. M. Otrokov, and E. V. Chulkov, “Competing Rhombohedral and Monoclinic Crystal Structures in MnPn_2Ch_4 Compounds: An Ab-Initio Study,” *J. Alloy Compd.* **709**, 172–178 (2017).
- [2] M M Otrokov, T V Menshchikova, M G Vergniory, I P Rusinov, A Yu Vyazovskaya, Yu M Koroteev, G Bihlmayer, A Ernst, P M Echenique, A Arnau, *et al.*,

- “Highly-Ordered Wide Bandgap Materials for Quantized Anomalous Hall and Magnetoelectric Effects,” *2D Mater.* **4**, 025082 (2017).
- [3] Mikhail M Otrokov, Ilya I Klimovskikh, Hendrik Bentmann, D Estyunin, Alexander Zeugner, Ziya S Aliev, S Gaß, AUB Wolter, AV Koroleva, Alexander M Shikin, *et al.*, “Prediction and Observation of an Antiferromagnetic Topological Insulator,” *Nature* **576**, 416–422 (2019).
- [4] E. D. L. Rienks, S. Wimmer, J. Sánchez-Barriga, O. Caha, P. S. Mandal, J. Růžička, A. Ney, H. Steiner, V. V. Volobuev, H. Groiss, *et al.*, “Large Magnetic Gap at the Dirac Point in $\text{Bi}_2\text{Te}_3/\text{MnBi}_2\text{Te}_4$ Heterostructures,” *Nature* **576**, 423–428 (2019).
- [5] Y. J. Chen, L. X. Xu, J. H. Li, Y. W. Li, H. Y. Wang, C. F. Zhang, H. Li, Y. Wu, A. J. Liang, C. Chen, *et al.*, “Topological Electronic Structure and Its Temperature Evolution in Antiferromagnetic Topological Insulator MnBi_2Te_4 ,” *Phys. Rev. X* **9**, 041040 (2019).
- [6] Yu-Jie Hao, Pengfei Liu, Yue Feng, Xiao-Ming Ma, Eike F. Schwier, Masashi Arita, Shiv Kumar, Chaowei Hu, Rui’e Lu, Meng Zeng, *et al.*, “Gapless Surface Dirac Cone in Antiferromagnetic Topological Insulator Bi_2Te_4 ,” *Phys. Rev. X* **9**, 041038 (2019).
- [7] Hang Li, Shun-Ye Gao, Shao-Feng Duan, Yuan-Feng Xu, Ke-Jia Zhu, Shang-Jie Tian, Jia-Cheng Gao, Wen-Hui Fan, Zhi-Cheng Rao, Jie-Rui Huang, *et al.*, “Dirac Surface States in Intrinsic Magnetic Topological Insulators EuSn_2As_2 and $\text{MnBi}_{2n}\text{Te}_{3n+1}$,” *Phys. Rev. X* **9**, 041039 (2019).
- [8] Przemyslaw Swatek, Yun Wu, Lin-Lin Wang, Kyungchan Lee, Benjamin Schruck, Jiaqiang Yan, and Adam Kaminski, “Gapless Dirac surface states in the antiferromagnetic topological insulator MnBi_2Te_4 ,” *Phys. Rev. B* **101**, 161109 (2020).
- [9] Chao Lei, Shu Chen, and Allan H MacDonald, “Magnetized Topological Insulator Multilayers,” *P. Natl. Acad. Sci. USA* **117**, 27224–27230 (2020).
- [10] Seng Huat Lee, Yanglin Zhu, Yu Wang, Leixin Miao, Timothy Pillsbury, Hemian Yi, Susan Kempinger, Jin Hu, Colin A Heikes, P Quarterman, *et al.*, “Spin Scattering and Noncollinear Spin Structure-Induced Intrinsic Anomalous Hall Effect in Antiferromagnetic Topological Insulator MnBi_2Te_4 ,” *Phys. Rev. Res.* **1**, 012011 (2019).
- [11] Yujun Deng, Yijun Yu, Meng Zhu Shi, Zhongxun Guo, Zihan Xu, Jing Wang, Xian Hui Chen, and Yuanbo Zhang, “Quantum Anomalous Hall Effect in Intrinsic Magnetic Topological Insulator MnBi_2Te_4 ,” *Science* **367**, 895–900 (2020).
- [12] Yan Gong, Jingwen Guo, Jiaheng Li, Kejing Zhu, Menghan Liao, Xiaozhi Liu, Qinghua Zhang, Lin Gu, Lin Tang, Xiao Feng, *et al.*, “Experimental Realization of an Intrinsic Magnetic Topological insulator,” *Chinese Phys. Lett.* **36**, 076801 (2019).
- [13] Dongqin Zhang, Minji Shi, Tongshuai Zhu, Dingyu Xing, Haijun Zhang, and Jing Wang, “Topological Axion States in the Magnetic Insulator MnBi_2Te_4 with the Quantized Magnetoelectric Effect,” *Phys. Rev. Lett.* **122**, 206401 (2019).
- [14] Ilya I Klimovskikh, Mikhail M Otrokov, Dmitry Estyunin, Sergey V Eremeev, Sergey O Filnov, Alexandra Koroleva, Eugene Shevchenko, Vladimir Voroshnin, Artem G Rybkin, Igor P Rusinov, *et al.*, “Tunable 3D/2D Magnetism in the $(\text{MnBi}_2\text{Te}_4)(\text{Bi}_2\text{Te}_3)_m$ Topological Insulators Family,” *npj Quantum Mater.* **5**, 1–9 (2020).

- [15] Jiaheng Li, Yang Li, Shiqiao Du, Zun Wang, Bing-Lin Gu, Shou-Cheng Zhang, Ke He, Wenhui Duan, and Yong Xu, “*Intrinsic Magnetic Topological Insulators in van der Waals Layered MnBi₂Te₄-Family Materials*,” *Sci. Adv.* **5**, eaaw5685 (2019).
- [16] Sugata Chowdhury, Kevin F. Garrity, and Francesca Tavazza, “*Prediction of Weyl semimetal and Antiferromagnetic Topological Insulator Phases in Bi₂MnSe₄*,” *npj Comput. Mater.* **5**, 33 (2019).
- [17] Bing Li, J-Q Yan, Daniel M Pajerowski, Elijah Gordon, A-M Nedić, Y Sizyuk, Liqin Ke, Peter P Orth, David Vaknin, and Robert J McQueeney, “*Competing Magnetic Interactions in the Antiferromagnetic Topological Insulator MnBi₂Te₄*,” *Phys. Rev. Lett.* **124**, 167204 (2020).
- [18] J-Q Yan, Qiang Zhang, Thomas Heitmann, Zengle Huang, KY Chen, J-G Cheng, Weida Wu, David Vaknin, Brian C Sales, and Robert John McQueeney, “*Crystal Growth and Magnetic Structure of MnBi₂Te₄*,” *Phys. Rev. Materials* **3**, 064202 (2019).
- [19] Alexander Zeugner, Frederik Nietschke, Anja U. B. Wolter, Sebastian Gaß, Raphael C. Vidal, Thiago R. F. Peixoto, Darius Pohl, Christine Damm, Axel Lubk, Richard Hentrich, *et al.*, “*Chemical Aspects of the Candidate Antiferromagnetic Topological Insulator MnBi₂Te₄*,” *Chem. Mater.* **31**, 2795–2806 (2019).
- [20] Jiazhen Wu, Fucai Liu, Masato Sasase, Koichiro Ienaga, Yukiko Obata, Ryu Yukawa, Koji Horiba, Hiroshi Kumigashira, Satoshi Okuma, Takeshi Inoshita, *et al.*, “*Natural van der Waals Heterostructural Single Crystals with both Magnetic and Topological Properties*,” *Sci. Adv.* **5**, eaax9989 (2019).
- [21] Shuai Zhang, Rui Wang, Xuepeng Wang, Boyuan Wei, Bo Chen, Huaqiang Wang, Gang Shi, Feng Wang, Bin Jia, Yiping Ouyang, *et al.*, “*Experimental Observation of the Gate-Controlled Reversal of the Anomalous Hall Effect in the Intrinsic Magnetic Topological Insulator MnBi₂Te₄ Device*,” *Nano Lett.* **20**, 709–714 (2019).
- [22] M. M. Otrokov, I. P. Rusinov, M. Blanco-Rey, M. Hoffmann, A. Yu. Vyazovskaya, S. V. Eremeev, A. Ernst, P. M. Echenique, A. Arnau, and E. V. Chulkov, “*Unique Thickness-Dependent Properties of the van der Waals Interlayer Antiferromagnet MnBi₂Te₄ Films*,” *Phys. Rev. Lett.* **122**, 107202 (2019).
- [23] Chang Liu, Yongchao Wang, Hao Li, Yang Wu, Yaixin Li, Jiaheng Li, Ke He, Yong Xu, Jinsong Zhang, and Yayu Wang, “*Robust Axion Insulator and Chern Insulator Phases in a Two-Dimensional Antiferromagnetic Topological Insulator*,” *Nat. Mater.* **19**, 522–527 (2020).
- [24] K. Y. Chen, B. S. Wang, J.-Q. Yan, D. S. Parker, J.-S. Zhou, Y. Uwatoko, and J.-G. Cheng, “*Suppression of the Antiferromagnetic Metallic State in the Pressurized MnBi₂Te₄ single Crystal*,” *Phys. Rev. Mater.* **3**, 094201 (2019).
- [25] Lei Ding, Chaowei Hu, Feng Ye, Erxi Feng, Ni Ni, and Huibo Cao, “*Crystal and Magnetic Structures of Magnetic Topological Insulators MnBi₂Te₄ and MnBi₄Te₇*,” *Phys. Rev. B* **101**, 020412 (2020).
- [26] Raphael C. Vidal, Alexander Zeugner, Jorge I. Facio, Rajyavardhan Ray, M. Hossein Haghghi, Anja U. B. Wolter, Laura T. Corredor Bohorquez, Federico Caglieris, Simon Moser, Tim Figgemeier, *et al.*, “*Topological Electronic Structure and Intrinsic Magnetization in MnBi₄Te₇: A Bi₂Te₃ Derivative with a Periodic Mn Sublattice*,” *Phys. Rev. X* **9**, 041065 (2019).
- [27] R. C. Vidal, H. Bentmann, T. R. F. Peixoto, A. Zeugner, S. Moser, C.-H. Min, S. Schatz, K. Kißner, M. Ünzelmann, C. I. Fornari, *et al.*, “*Surface States and Rashba-Type Spin Polarization in Antiferromagnetic MnBi₂Te₄(0001)*,” *Phys. Rev. B* **100**, 121104 (2019).
- [28] Jun Ge, Yanzhao Liu, Jiaheng Li, Hao Li, Tianchuang Luo, Yang Wu, Yong Xu, and Jian Wang, “*High-Chern-Number and High-Temperature Quantum Hall Effect Without Landau Levels*,” *Natl. Sci. Rev.* **7**, 1280–1287 (2020).
- [29] Andrew M. Essin, Joel E. Moore, and David Vanderbilt, “*Magnetoelectric Polarizability and Axion Electrodynamics in Crystalline Insulators*,” *Phys. Rev. Lett.* **102**, 146805 (2009).
- [30] Roger S. K. Mong, Andrew M. Essin, and Joel E. Moore, “*Antiferromagnetic topological insulators*,” *Phys. Rev. B* **81**, 245209 (2010).
- [31] Haiming Deng, Zhiyi Chen, Agnieszka Woloś, Marcin Konczykowski, Kamil Sobczak, Joanna Sitnicka, Irina V Fedorchenko, Jolanta Borysiuk, Tristan Heider, Łukasz Pluciński, *et al.*, “*High-Temperature Quantum Anomalous Hall Regime in a MnBi₂Te₄/Bi₂Te₃ Superlattice*,” *Nat. Phys.* **17**, 36–42 (2020).
- [32] Dmitry Ovchinnikov, Xiong Huang, Zhong Lin, Zaiyao Fei, Jiaqi Cai, Tiancheng Song, Minhao He, Qianni Jiang, Chong Wang, Hao Li, *et al.*, “*Intertwined Topological and Magnetic Orders in Atomically Thin Chern Insulator MnBi₂Te₄*,” arXiv preprint arXiv:2011.00555 (2020).
- [33] Shiqi Yang, Xiaolong Xu, Yaozheng Zhu, Ruirui Niu, Chungqiang Xu, Yuxuan Peng, Xing Cheng, Xionghui Jia, Yuan Huang, Xiaofeng Xu, *et al.*, “*Odd-Even Layer-Number Effect and Layer-Dependent Magnetic Phase Diagrams in MnBi₂Te₄*,” *Phys. Rev. X* **11**, 011003 (2020).
- [34] Olav Hellwig, Taryl L Kirk, Jeffrey B Kortright, Andreas Berger, and Eric E Fullerton, “*A New Phase Diagram for Layered Antiferromagnetic Films*,” *Nat. Mater.* **2**, 112–116 (2003).
- [35] Ulrich K Rößler and Alexei N Bogdanov, “*Reorientation in Antiferromagnetic Multilayers: Spin-Flop Transition and Surface Effects*,” *Phys. Status Solidi (C)* **1**, 3297–3305 (2004).
- [36] Björn Skubic, Johan Hellsvik, Lars Nordström, and Olle Eriksson, “*A Method for Atomistic Spin Dynamics Simulations: Implementation and Examples*,” *J. Phys.: Condens. Mat.* **20**, 315203 (2008).
- [37] Richard F L Evans, Weijia J Fan, Phanwadee Chureemart, Thomas A Ostler, Matthew O A Ellis, and Roy W Chantrell, “*Atomistic Spin Model Simulations of Magnetic Nanomaterials*,” *J. Phys.: Condens Mat.* **26**, 103202 (2014).
- [38] Paul M Sass, Jinwoong Kim, David Vanderbilt, Jiaqiang Yan, and Weida Wu, “*Robust A-Type Order and Spin-Flop Transition on the Surface of the Antiferromagnetic Topological Insulator MnBi₂Te₄*,” *Phys. Rev. Lett.* **125**, 037201 (2020).
- [39] Aoyu Tan, Valentin Labracherie, Narayan Kunchur, Anja UB Wolter, Joaquin Cornejo, Joseph Dufouleur, Bernd Büchner, Anna Isaeva, and Romain Giraud, “*Metamagnetism of Weakly Coupled Antiferromagnetic Topological Insulators*,” *Phys. Rev. Lett.* **124**, 197201 (2020).
- [40] Jiazhen Wu, Fucai Liu, Can Liu, Yong Wang, Changcun Li, Yangfan Lu, Satoru Matsuishi, and Hideo Hosono,

- “*Toward 2D Magnets in the $(\text{MnBi}_2\text{Te}_4)(\text{Bi}_2\text{Te}_3)_n$ Bulk Crystal*,” *Adv. Mater.* **32**, 2001815 (2020).
- [41] D L Mills, “*Surface Spin-Flop State in a Simple Antiferromagnet*,” *Phys. Rev. Lett.* **20**, 18 (1968).
- [42] Chao Lei and Allan H. MacDonald, “*Gate-Tunable Quantum Anomalous Hall Effects in MnBi_2Te_4 Thin Films*,” arXiv preprint arXiv:2101.07181 (2021).
- [43] Ryogo Kubo, “*Statistical-Mechanical Theory of Irreversible Processes. I. General Theory and Simple Applications to Magnetic and Conduction Problems*,” *J.Phys. Soc. Jpn/* **12**, 570–586 (1957).
- [44] D A Greenwood, “*The Boltzmann Equation in the Theory of Electrical Conduction in Metals*,” *Proc. Phys. Soc. (1958-1967)* **71**, 585 (1958).
- [45] Wang-Kong Tse and A. H. MacDonald, “*Magneto-optical Faraday and Kerr Effects in Topological Insulator Films and in Other Layered Quantized Hall Systems*,” *Phys. Rev. B* **84**, 205327 (2011).